

## Supporting Information

---

### ESIPT and FRET Probes for Monitoring Nanoparticle Polymer Coating Stability

Julio. C. Azcárate<sup>a</sup>, Sebastián A. Díaz<sup>b</sup>, Jonathan A. Fauerbach<sup>c</sup>, Florencia Gillanders<sup>b</sup>, Aldo A. Rubert<sup>a</sup>, Elizabeth A. Jares-Erijman<sup>c‡</sup>, Thomas M. Jovin<sup>b</sup>, Mariano H. Fonticelli<sup>a</sup>

- a. Instituto de Investigaciones Fisicoquímicas Teóricas y Aplicadas (INIFTA), Facultad de Ciencias Exactas, Universidad Nacional de La Plata - CONICET Sucursal 4, Casilla de Correo 16, 1900 La Plata, Argentina.
  - b. Laboratory of Cellular Dynamics, Max Planck Institute for Biophysical Chemistry, Am Fassberg 11, 37077, Göttingen, Germany.
  - c. Departamento de Química Orgánica, Facultad de Ciencias Exactas y Naturales, Universidad de Buenos Aires, 1428 Buenos Aires, Argentina. ‡Deceased Sept. 29, 2011.
- 

### Contents

SI- 1.	TEM – Size distribution of AuNPs .....	2
SI- 1.	Agarose Gel Electrophoresis.....	2
SI- 2.	Comparison of purification methods for coated-AuNP.....	3
SI- 3.	ESIPT process.....	5
SI- 4.	ESIPT Spectra Deconvolution Procedure .....	7
SI- 5.	PMA-FE-C12N polymersomes spectra upon addition of i-PrOH. ....	8
SI- 6.	AuNP@PMA-FC-C12N spectra upon addition of several cosolvents.....	9

## SI- 1. TEM – Size distribution of AuNPs

Dodecanethiol capped AuNPs were synthesized by exploiting the two-phase Brust-Schiffrin method. Different size distributions were achieved by adjusting the thiol-gold ratio during the synthesis.<sup>1</sup> The size distribution was characterized by transmission electron microscopy (TEM) using a Phillips CM200 UT microscope operating at 200kV in bright field condition, and fitting the histogram with a lognormal curve.<sup>2</sup> The AuNPs were further characterized by UV-vis spectroscopy.

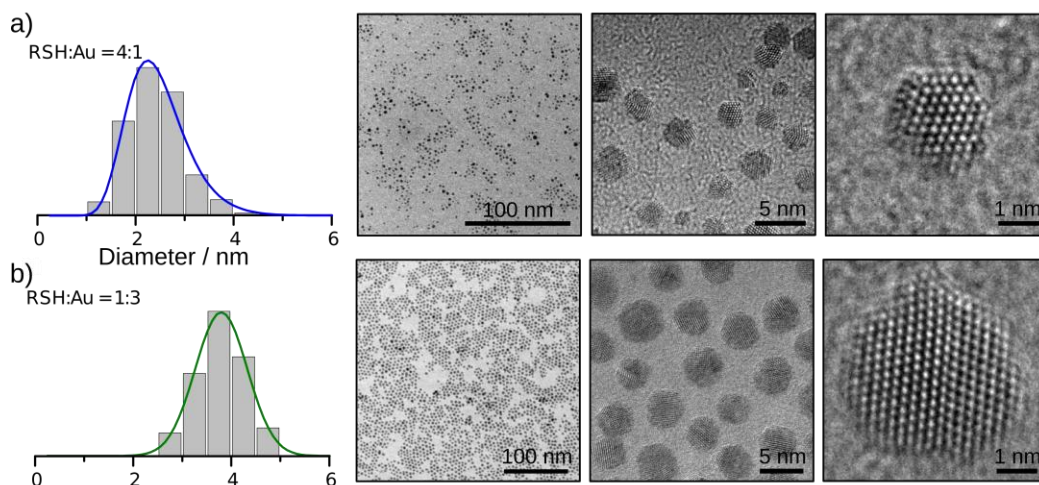


Figure SI 1: Characterization of dodecanethiol capped AuNPs by TEM under Bright Filed conditions and HRTEM. The AuNPs labeled as 2 and 4 nm had a mean diameter of  $2.5 \pm 0.6$  nm and  $3.9 \pm 0.6$  nm, respectively.

## SI- 1. Agarose Gel Electrophoresis

We evaluated different methods for coated-AuNP purification focusing on the removal of the unassembled polymer (polymersomes). Agarose gel (1% p/v) electrophoresis in 1x TBE buffer using a field of 10V/cm), a procedure used conventionally for DNA purification, was found to be appropriate for the amount of sample to be purified.

The gels were prepared with several sample wells of 400  $\mu$ L. The unpurified coated-AuNP dispersed in 1x TBE were applied to the wells. After  $\sim$ 30 min of electrophoresis the two bands (coated-AuNP and polymersomes) were resolved. The 4 nm coated-AuNPs were visible by eye, and the smaller NPs were revealed by UV light (365 nm) excitation of the the FC dye in the polymer coating (Figure S2a).

To recover the purified coated-AuNP from the agarose gel we followed the following procedure. First, each agarose gel fraction containing the purified coated-AuNP was cut out. The gel fractions were placed inside cellulose dialysis tubes (MWCO 3.5K Da), which were filled with 400 $\mu$ L fresh TEB 1x buffer solution, sealed by clamping, and placed inside an electrophoresis cell operated at the same field as above, until all the coated-AuNP were eluted from the gel fragment (Figure S2b).

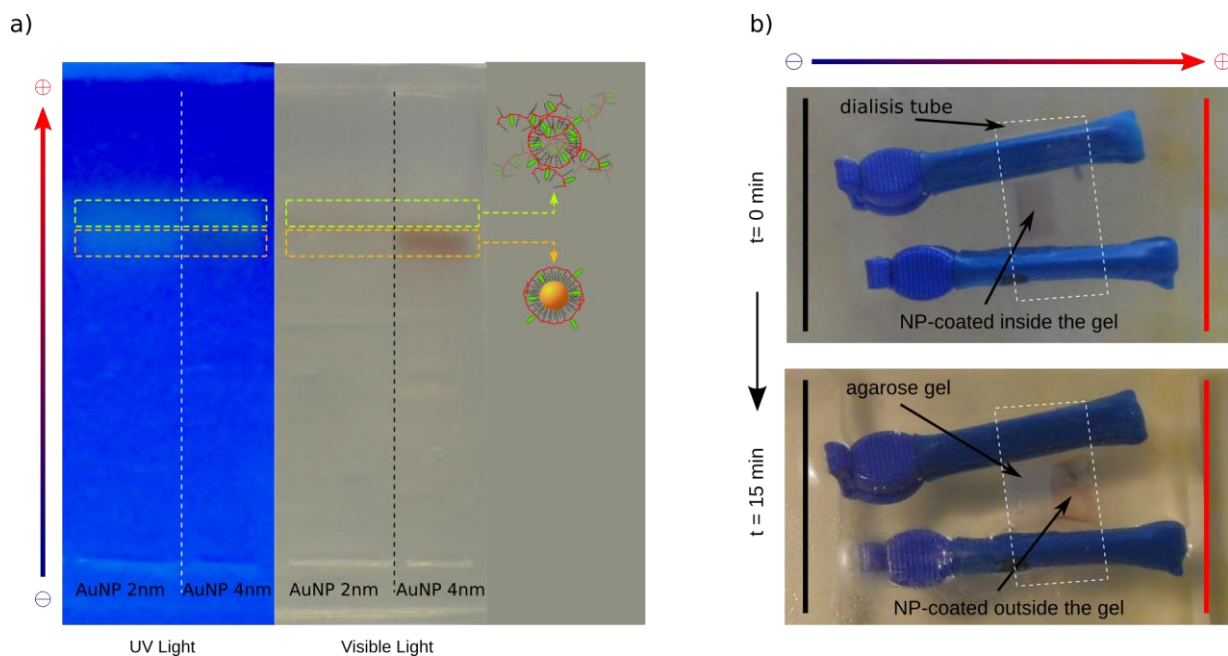


Figure S2:a) Purification by agarose gel electrophoresis and b) recovery of products by electro-elution inside a dialysis tube (MWCO 3.5 KDa).

## SI- 2. Comparison of purification methods for coated-AuNP

A portion of the same batch of coated-AuNPs was purified by size exclusion chromatography using a Superdex 200 analytical column (GE Healthcare Life Science) in an HPLC system with three-wavelength UV-vis detection. Elution was started with 1× TBE buffer and a flow of 50  $\mu\text{L}/\text{min}$  for 3 min, and then 20  $\mu\text{L}/\text{min}$ . The average run time was 80 min. A set of fractions were collected, and their fluorescence and absorption spectra were measured. For each fraction Dynamic Light Scattering (DLS) was used to characterize the size of coated-AuNP or polymersomes. It was found that the fractions corresponding to polymersomes or coated-AuNP had the same nominal size and distribution irrespective of the purification method (Figure S3a). In Figure S3b the maximal plasmonic absorbance of AuNPs at 520 nm and the fluorescence intensity of FC probes at 550 nm ( $T^*$  band) are represented for the eluted fraction. The polymersomes, smaller in size, had the greatest mobility in agarose gel electrophoresis and migrated further than coated-AuNP (Figure S2a). Accordingly, they constituted the “slowest” fraction in size exclusion chromatography (Figure Sb)

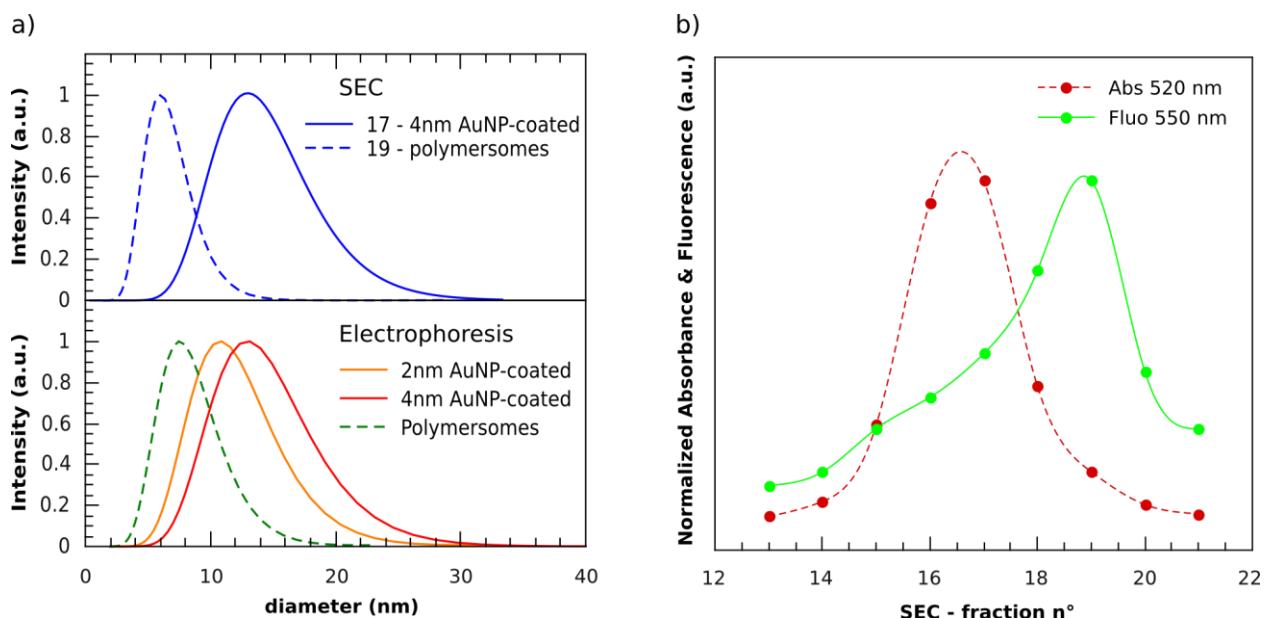


Figure S3: a) Dynamic Light Scattering Intensity for samples fractionized by Size Exclusion Chromatography and Agarose Electrophoresis. b) Absorbance of AuNP (520 nm) and Fluorescence of FC (550 nm) for the fractions eluted in size exclusion chromatography.

Scanning Electronic Microscopy (SEM) images of the coated-AuNPs purified by agarose gel electrophoresis were taken to corroborate the size of the assemblies (Figure S4). Due to sample carbonization the acquisition of high-quality images was difficult, even operating the microscope at low electron acceleration. The images show spheres of sizes compatible with the DLS results.

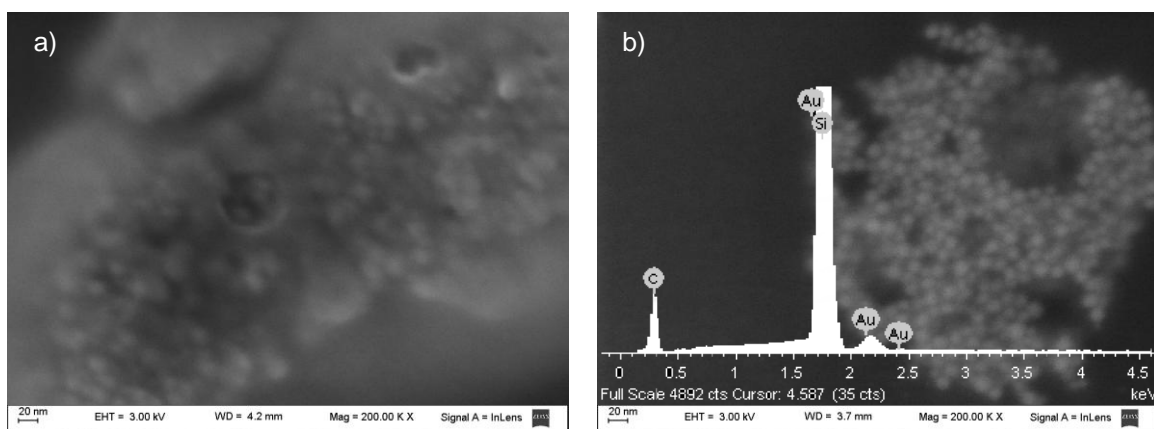


Figure S4: SEM images acquired at 3kV. a) An area with sample carbonization even at low electron acceleration. b) A fresh zone of the sample prior to carbonization. The observed spheres had sizes between 10-20nm. The EDS spectrum (inset) confirmed the presence of gold.

Recently, it has been reported by Parak and colleagues that the best purification method for these kind of systems is ultracentrifugation.<sup>3</sup> In our study agarose gel electrophoresis was satisfactory, as it allowed a reasonable separation between the coated-AuNPs and the polymersomes. Additionally control experiments with  $\text{CHCl}_3$  demonstrated that the free polymer was not in excessive concentrations. In Figure S5 it can be seen that the fluorescence spectrum of the polymersome fraction was very different than that of coated-AuNPs, confirming the successful purification of

the coated-AuNPs. The differences in the behavior of coated-AuNPs and polymersomes upon i-PrOH addition, detailed in section SI-5, support this conclusion.

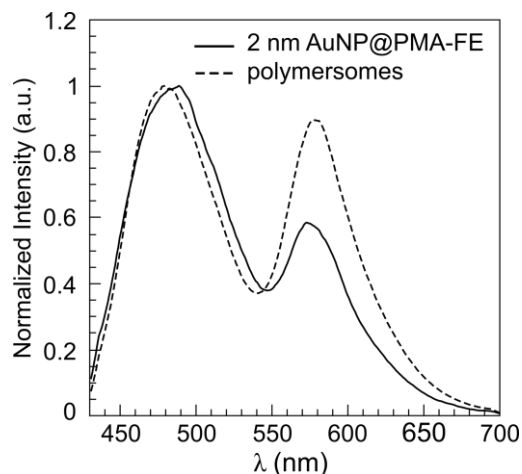
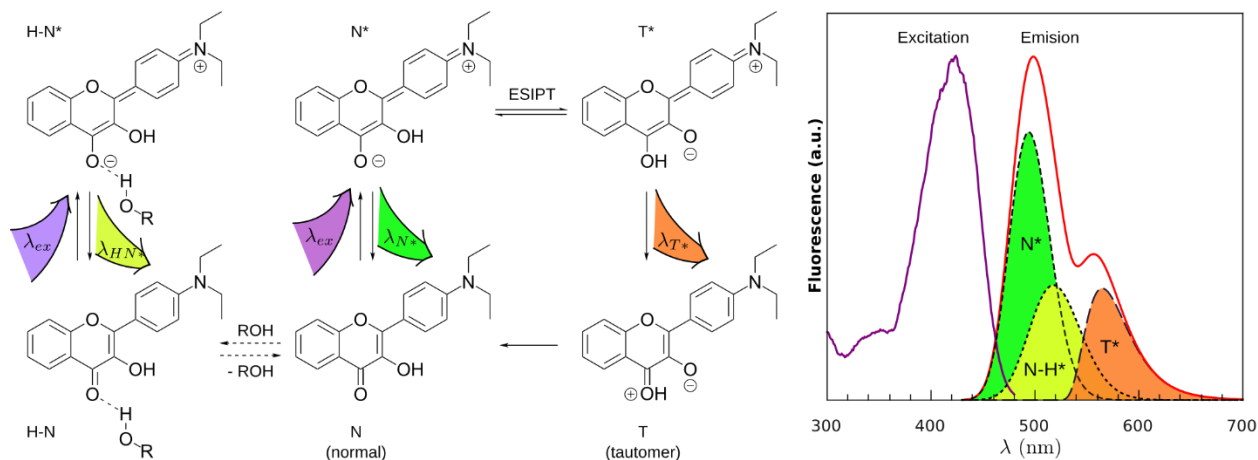


Figure S5: Fluorescence spectra of coated-AuNP (filled line) and unassembled polymersomes (dashed line) separated by agarose gel electrophoresis.

### SI- 3. ESIPT process

Scheme S1 shows the photochemical process for triple fluorescence emission of ESIPT probes. The  $N^*$  and  $T^*$  bands reflect the ESIPT phenomenon in the excited state and the third band is due to intermolecular interaction with protic molecules in the ground state.



Scheme S1 : Photochemistry/photophysics of ESIPT process and excitation-emission spectra with their corresponding deconvolution

In the case of the FE probe the aniline group bonded at position 2 induces a strong charge transfer effect which increases the intermolecular interaction of the dye with protic molecules ( $H_2O$  or alcohol). This effect is observed as a red shift in the band with shortest wavelength. That unresolved broad band was deconvoluted by introducing a third band representing the intermolecular interaction with protic solvents.<sup>4,5</sup>

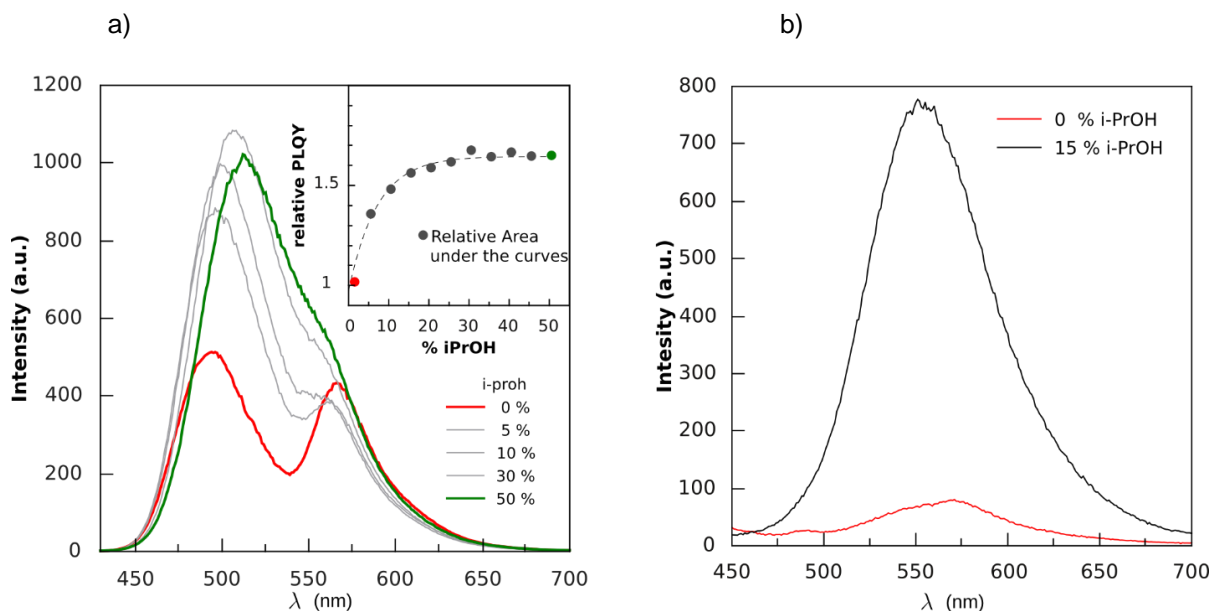


Figure S6: Spectra of AcFE in a)  $\text{CHCl}_3$  and b)  $\text{H}_2\text{O}$ , and their mixtures with i-PrOH.

Figure S6 shows the spectra of the AcFE probe in  $\text{CHCl}_3$  and  $\text{H}_2\text{O}$  for increasing fractions of i-PrOH. In

Figure S6a a red shift in the low wavelength band and a great increase in PLQY (or total fluorescence) were observed, also occurred. In the case of AcFE in  $\text{H}_2\text{O}$  (

Figure S6b) the ESIPT process was completely absent, and the PLQY was very low. The addition of i-PrOH led to a dramatic increase in total fluorescence but ESIPT was not apparent.

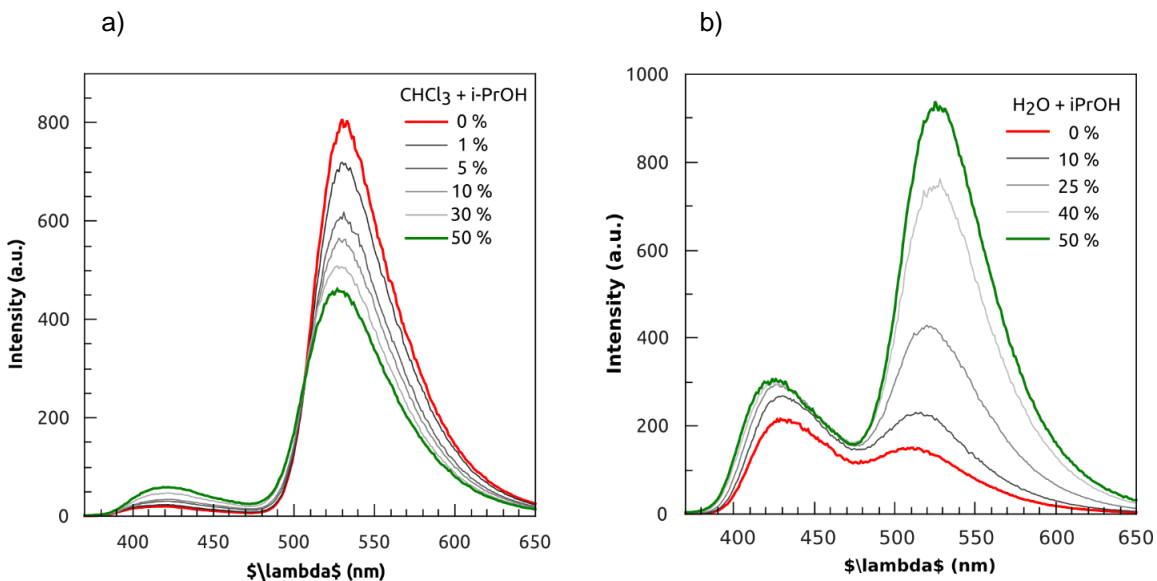


Figure S7: Spectra of AcFC in a)  $\text{CHCl}_3$  and b)  $\text{H}_2\text{O}$  with increasing fractions of i-PrOH

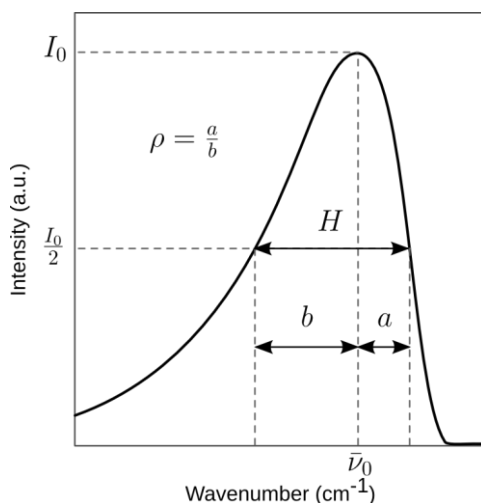
In contrast with AcFE, no significant shift in band positions were observed for AcFC upon addition of *i*-PrOH (Figure S7). This result is attributed to the absence of an H-N\* band in AcFC due to the smaller charge transfer of the furyl group compared to the N,N-diethylaminophenyl in AcFE.

## SI- 4. ESIPT Spectra Deconvolution Procedure

The spectra were deconvoluted using an approximation of the four parameters asymmetric LogNormal function of Siano-Metzler<sup>5,6</sup>

$$\text{alogn}(\bar{\nu}_0, H, \rho, I_0, \bar{\nu}) = I_0 \exp \left[ - \left( \frac{\ln 2}{(\ln \rho)^2} \right) \left( \ln \left[ \left( \frac{\bar{\nu} - \bar{\nu}_0}{H} \right) \left( \frac{\rho^2 - 1}{\rho} \right) + 1 \right] \right)^2 \right]$$

where the  $\bar{\nu}_0, H, \rho$  and  $I_0$  are defined in the figure below



We used the open source software *Fityk7* to deconvolute the spectra and rewrote the above equation as an approximation:

$$\text{LogNormal}(\bar{\nu}_0, H, B, I_0, \bar{\nu}) = I_0 \exp \left[ - \ln 2 \left( \frac{\ln \left[ 2B \left( \frac{\bar{\nu} - \bar{\nu}_0}{H} \right) + 1 \right]}{B} \right)^2 \right]$$

where  $\left( \frac{\rho^2 - 1}{\rho} \right) \approx 2 \ln \rho \Rightarrow B = \ln \rho$ .

In accordance with Caarls *et.al*<sup>6</sup>, the peak's asymmetry was restricted to  $0.5 \leq \rho \leq 1$ , which translates to  $-0.7 \leq B \leq 0$  in the approximated function.

The algorithm used to find the proper position and shape of each band was:

1. For 0% *i*-PrOH, only two peaks were fit, obtaining approximated values for position ( $\bar{\nu}_0$ ) and shape ( $H, B$ ).
2. For 50% *i*-PrOH, two peaks were added after fixing the values for  $\bar{\nu}_0, H$  and  $B$  obtained above. A third peak was then added and fitted.

- For a 25% *i*-PrOH we used the parameters obtained in 2 for the three bands, and fitting fixing  $\bar{\nu}_0$ ,  $H$  and  $B$ . The  $H$  values were fit after fixing the values obtained for  $I_0$ . With the values obtained in the steps above, every spectra for each % *i*-PrOH were fitted with just  $I_0$  as a free parameter.
- Finally, all fits were repeated iteratively, each time with one free parameter ( $I_0 \rightarrow \bar{\nu}_0 \rightarrow H \rightarrow B \rightarrow I_0 \dots$ ). The last fits were carried out with with free parameters.

Table S1 shows the parameters obtained after deconvolution of spectra for AcFE probes in  $\text{CHCl}_3$  upon addition of *i*-PrOH. Figure S shows the spectral deconvolution for AcFE, clearly indicating the increase in H-N\* with *i*-PrOH due to protic intermolecular interaction. This increase in the H-N\* band is reflected as red shift in the first unresolved band.

Table S1: Parameters obtained by fitting AcFE spectra in  $\text{CHCl}_3$  with addition of *i*-PrOH.

Component	$\bar{\nu}_0$ ( $\text{cm}^{-1}$ )	$H$ ( $\text{cm}^{-1}$ )	$\rho$	$\lambda_0$ (nm)	fwhm (nm)
N*	20325	1960	0.8	492	47
H-N*	19342	2170	0.75	517	57
T*	17699	1340	0.65	565	42

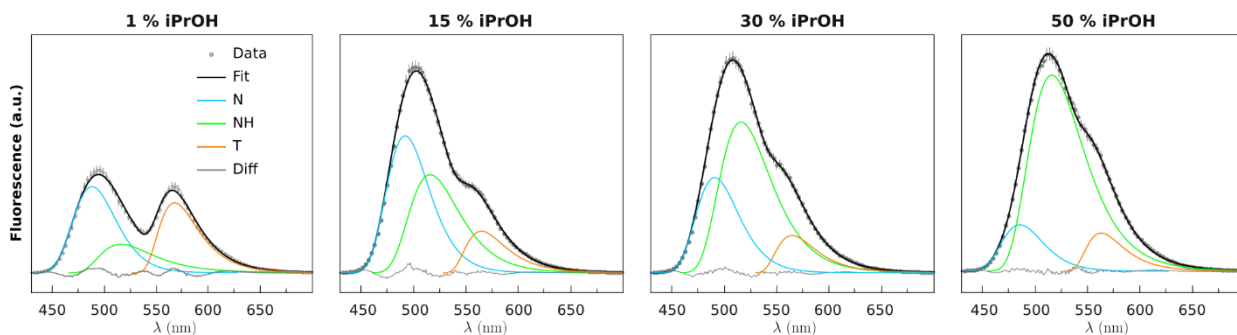


Figure S8: Three-Band Spectra deconvolution for AcFE probes in  $\text{CHCl}_3$  with increasing amounts of *i*-PrOH.

## SI- 5. PMA-FE-C12N polymersomes spectra upon addition of *i*-PrOH.

As in the experiments realized in the main text the behavior of unassembled PMA-FE-C12 strands were tested by successive addition of *i*-PrOH. The unassembled polymersomes were recovered from the agarose gel in the same way as coated-AuNPs. Figure S9 show the fluorescence spectra for different *i*-PrOH concentration in two different pH media. Clearly the behavior of polymersomes is much more erratic than that of the coated-AuNPs (compare with Fig. 2 and Fig. 5b in the main paper). It is interesting to note that the PLQY of the polymersomes at pH 8.5 decreased constantly. However, for the assemblies AuNP@PMA-FE the PLQY decreased with the first addition of *i*PrOH and then increased (see Figure 2 in the main paper). Also, the behavior at pH 7.4 was different for polymersomes with respect to AuNP@PMA-FE (compare with Figure 5b in the main paper). For polymersomes at pH 7.4 the PLQY decreased with the first addition of *i*-PrOH and then increase, although Figure 5b indicates that the fluorescence signal increased constantly for AuNP@PMA-FE at the same pH.

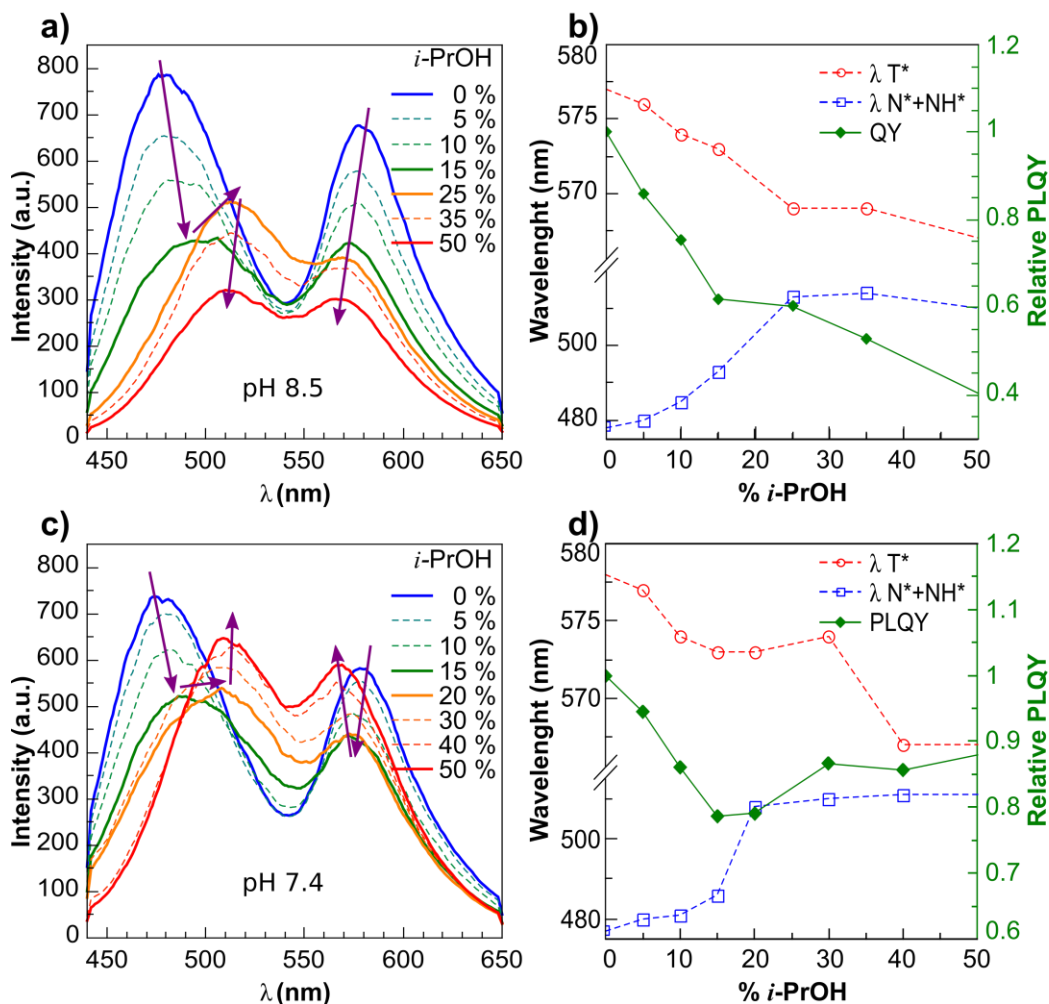


Figure S9: Fluorescence spectra of PMA-FC-C12N polymersomes upon *i*-PrOH addition at different pHs: a) at pH 8.5 (TBE buffer) and c) at pH 7.4. Panels (b,d) show the relative PLQY and the band shifts for the spectra on the left.

## SI- 6. AuNP@PMA-FC-C12N spectra upon addition of several cosolvents

The fluorescence spectra of the AuNP-containing buffer solutions were recorded after each addition of cosolvent (Figure S10 a-d). In all cases, the  $N^*$  band intensity increased with cosolvent addition. It is important to note that the light scattering can contribute to the apparent fluorescence intensity in the  $N^*$  region, especially for aprotic solvents. On the other hand, the  $T^*$  band intensity decreased with the first cosolvent additions and then increased for the most of the cosolvents. For MeCN (d) only the increase in  $T^*$  was observed. The band ratio ( $I_{N^*}/I_{T^*}$ ) clearly shows how the media polarity changed upon cosolvent addition (Figure S9 (e, f)). Drastic changes in behavior were observed within a similar range of solvent content. The break points at 20-30% of cosolvent indicate a change in ES IPT probe location (microenvironment) and are attributed to polymer stripping. The increase in light scattering is also an indication of polymer stripping, which is more significant for > 20% of added cosolvent.

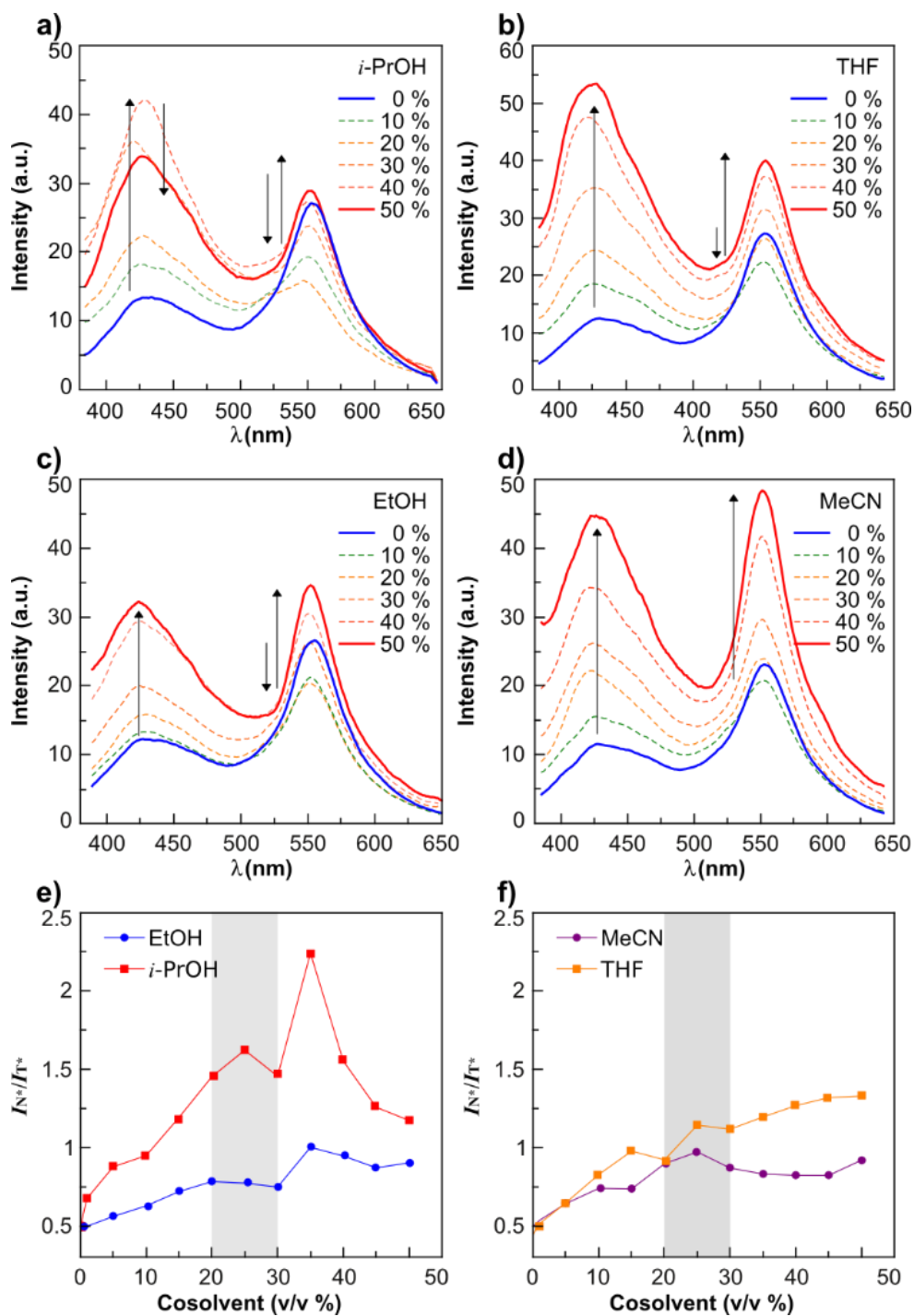


Figure S10: Spectra of AuNP@PMA-FC-NC12 upon addition of: a) *i*-propanol, b) tetrahydrofuran, c) ethanol and d) acetonitrile. e) and f) show the  $I_N^+/I_T^*$  for protic and aprotic cosolvent added.

## References

- 1 M. J. Hostetler, J. E. Wingate, C.-J. Zhong, J. E. Harris, R. W. Vachet, M. R. Clark, J. D. Londono, S. J. Green, J. J. Stokes, G. D. Wignall, G. L. Glish, M. D. Porter, N. D. Evans and R. W. Murray, *Langmuir*, 1998, **14**, 17–30.
- 2 C. G. Granqvist, *J. Appl. Phys.*, 1976, **47**, 2200.
- 3 J. Hühn, C. Carrillo-Carrion, M. G. Soliman, C. Pfeiffer, D. Valdeperez, A. Masood, I. Chakraborty, L. Zhu, M. Gallego, Z. Yue, M. Carril, N. Feliu, A. Escudero, A. M. Alkilany, B. Pelaz, P. del Pino and W. J. Parak, *Chem. Mater.*, 2017, **29**, 399–461.
- 4 M. S. Celej, W. Caarls, A. P. Demchenko and T. M. Jovin, *Biochemistry*, 2009, **48**, 7465–7472.
- 5 W. Caarls, M. Soledad Celej, A. P. Demchenko and T. M. Jovin, *J. Fluoresc.*, 2010, **20**, 181–90.
- 6 D. B. Siano, *J. Chem. Phys.*, 1969, **51**, 1856.
- 7 M. Wojdyr, *J. Appl. Crystallogr.*, 2010, **43**, 1126–1128.